arXiv:1910.10635v1 [quant-ph] 18 Oct 2019

One-step implementation of a multi-target-qubit controlled phase gate with cat-state qubits in circuit QED

You-Ji Fan[1], Zhen-Fei Zheng[2], Yu Zhang[3], Dao-Ming Lu[1], and Chui-Ping Yang[4,5*]

[1] *College of Mechanic and Electronic Engineering, Wuyi University, Wuyishan 354300, Fujiang, China*

[2] *CAS Key Laboratory of Quantum Information, University of Science and Technology of China, Hefei 230026, China*

[3] *School of Physics, Nanjing University, Nanjing 210093, China*

[4] *Quantum Information Research Center, Shangrao Normal University, Shangrao 334001, China and*

[5] *Department of Physics, Hangzhou Normal University, Hangzhou 310036, China*

Abstract

We propose a single-step implementation of a muti-target-qubit controlled phase gate with one cat-state qubit (*cqubit*) simultaneously controlling $n-1$ target *cqubits*. The two logic states of a *cqubit* are represented by two orthogonal cat states of a single cavity mode. In this proposal, the gate is implemented with n microwave cavities coupled to a superconducting transmon qutrit. Because the qutrit remains in the ground state during the gate operation, decoherence caused due to the qutrit's energy relaxation and dephasing is greatly suppressed. The gate implementation is quite simple because only a single-step operation is needed and neither classical pulse nor measurement is required. Numerical simulations demonstrate that high-fidelity realization of a controlled phase gate with one cqubit simultaneously controlling two target cqubits is feasible with present circuit QED technology. This proposal can be extended to a wide range of physical systems to realize the proposed gate, such as multiple microwave or optical cavities coupled to a natural or artificial three-level atom.

PACS numbers:

*Electronic address: yangcp@hznu.edu.cn

I. INTRODUCTION

Quantum computing has attracted considerable interest since quantum computers can solve hard computational problems much more efficiently than classical computers [1-3]. Multiqubit gates play an important role in quantum computing. It is known that a multiqubit gate can in principle be constructed with single-qubit and two-qubit basic gates. However, the methods based on the conventional gate-decomposition protocols [4-6] are complicated and not easy to implement experimentally. For instance, the number of universal two-qubit gates, which are needed to implement multiqubit gates, increases drastically with the number of qubits [4-6]. As a result, the operation time required for implementing a multiqubit gate would be quite long and thus the fidelity would be significantly deteriorated by decoherence. Hence, it is worthwhile to seek efficient approaches to realize multiqubit gates.

There exist two kinds of significant multiqubit gates, i.e., multiqubit gates with multiple control qubits acting on a single target qubit (also called multiqubit Toffoli gates or multi-control-qubit gates), and multiqubit gates with a single qubit simultaneously controlling multiple target qubits. For the past years, much progress has been made in the physical realization of these two types of multiqubit gates. Several schemes for realizing three-qubit Toffoli gates have been proposed with neutral atoms in an optical lattice [7] or hybrid atom-photon qubits [8]. In addition, experimental realization of a three-qubit controlled phase gate in NMR quantum system [9] and a three-qubit Toffoli gate with superconducting qubits [10] has been reported. On the other hand, based on cavity or circuit QED, many theoretical proposals have been presented for directly realizing not only multi-control-qubit gates [11-22] but also multi-target-qubit gates [23-27], in various physical qubits.

In recent years, cat-state qubits (*cqubits*), which are encoded with cat states, have drawn intensive attention due to their enhanced life times with quantum error correction (QEC). For instance, the lifetime of a cqubit can be made to be 2 up to 320 μs with QEC [28]. Recently, there is an increasing interest in quantum computing with cat-state encoding qubits. Several schemes have been presented for realizing single-cqubit gates and two-cqubit gates [29-31]. Moreover, single-cqubit gates [32] and two-cqubit entangled Bell states [33] have been experimentally implemented recently. In addition, the circuit QED, consisting of microwave cavities and artificial atoms, is particularly attractive and has been considered

as one of the leading candidates for quantum information processing [34-45].

The focus of this work is on a multi-target-qubit controlled phase gate with one qubit simultaneously controlling multiple target qubits. This multi qubit phase gate is described by

$$\begin{aligned} |0_1\rangle |i_2\rangle |i_3\rangle ... |i_n\rangle &\rightarrow |0_1\rangle |i_2\rangle |i_3\rangle ... |i_n\rangle , \\ |1_1\rangle |i_2\rangle |i_3\rangle ... |i_n\rangle &\rightarrow |1_1\rangle (-1)^{i_2} (-1)^{i_3} ... (-1)^{i_n} |i_2\rangle |i_3\rangle ... |i_n\rangle , \end{aligned} \tag{1}$$

where subscript 1 represents the control qubit while subscripts $2, 3, \ldots,$ and n represent target qubits, and $i_2, i_3, ...i_n \in \{0, 1\}$. Equation (1) implies that, when the control qubit is in the state $|0\rangle$, nothing happens to the states of each target qubit; however, when the control qubit is in $|1\rangle$, a phase flip (from sign + to −) happens to the state $|1\rangle$ of each target qubit. This multiqubit gate is useful in quantum computing and quantum information processing, such as in entanglement preparation [46], error correction [47], quantum algorithms [48], and quantum cloning [49]. After a deep search of the literature, we found that how to directly realize this multiqubit gate with cat-state qubits has not been reported yet.

Motivated by the above, we will propose a method to realize the multi-target-qubit controlled phase gate (1) with *cqubits*, by using n microwave cavities coupled to a superconducting transmon qutrit (a three-level artificial atom) (Fig. 1). This proposal is based on circuit QED. As shown below, this proposal has the following advantages. During the gate operation, the qutrit stays in the ground state. Thus, decoherence from the qutrit is greatly suppressed. The gate implementation is simple because of only one-step operation and no need of classical pulse or measurement. The gate operation time is independent of the number of the *cqubits*. Our numerical simulations show that high-fidelity implementation of a controlled phase with one cqubit simultaneously controlling two cqubits is feasible with current circuit QED technology. This proposal can be extended to a wide range of physical systems to realize the proposed gate, such as multiple microwave or optical cavities coupled to a natural or artificial three-level atom.

This paper is organized as follows. In Sec. II, we explicitly show how to realize a controlled-phase gate with one cqubit simultaneously controlling $n - 1$ target cqubits. In Sec. III, we give a brief discussion on the experimental feasibility of implementing a three-qubit controlled phase gate with one cqubit simultaneously controlling two target cqubits.

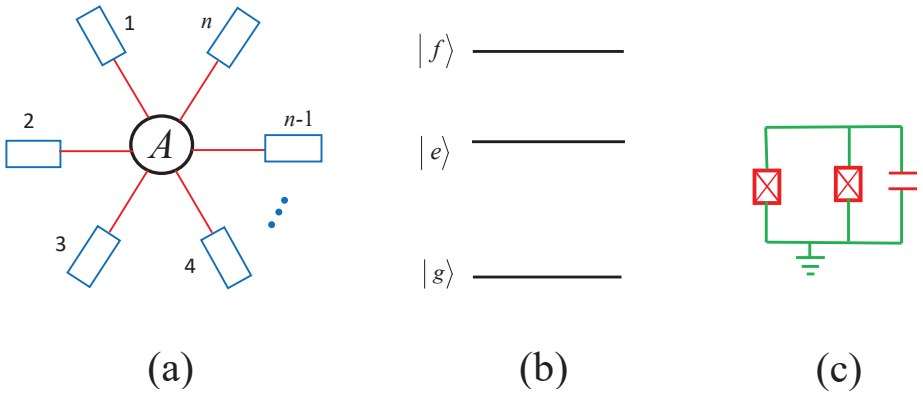


FIG. 1: (Color online) (a) Diagram of n cavities $(1, 2, ..., n)$ coupled to a superconducting transmon qutrit (A). A square represents a cavity, which can be one-dimensional or three-dimensional cavity. The qutrit is capacitively or inductively coupled to each resonator. (b) Level configuration of the transmon qutrit, for which the level spacing between the upper two levels is smaller than that between the two lowest levels. (c) Electronic circuit of a transmon qutrit, which consists of two Josephson junctions and a capacitor.

We end up with a conclusion in Sec. IV.

II. MULTI-TARGET-CQUBIT CONTROLLED PHASE GATE

Consider n microwave cavities $(1, 2, ..., n)$ coupled to a superconducting transmon qutrit [Fig. 1(a)]. The three level of the qutrit are denoted as $|g\rangle$, $|e\rangle$ and $|f\rangle$, as shown in Fig. 1(b). Theoretically, the $|g\rangle \leftrightarrow |f\rangle$ coupling for an ideal transmon is zero due to the selection rule [50]. However, in practice, there exists a weak coupling between the two levels $|g\rangle$ and $|f\rangle$ [51]. Suppose that cavity 1 is off-resonantly coupled to the $|g\rangle \leftrightarrow |e\rangle$ transition of the qutrit with coupling constant g_1 and detuning $|\delta_1|$ but highly detuned (decoupled) from the $|e\rangle \leftrightarrow |f\rangle$ transition of the qutrit. In addition, assume that cavity l $(l = 2, 3, ..., n)$ is off-resonantly coupled to the $|e\rangle \leftrightarrow |f\rangle$ transition of the qutrit with coupling constant g_l and detuning $|\delta_l|$ but highly detuned (decoupled) from the $|g\rangle \leftrightarrow |e\rangle$ transition of the qutrit (Fig. 2). Note that the coupling and decoupling conditions can in principle be satisfied by prior adjustment of the qutrit's level spacings or/and the cavity frequency. For a superconducting (SC) qutrit, the level spacings can be rapidly (within

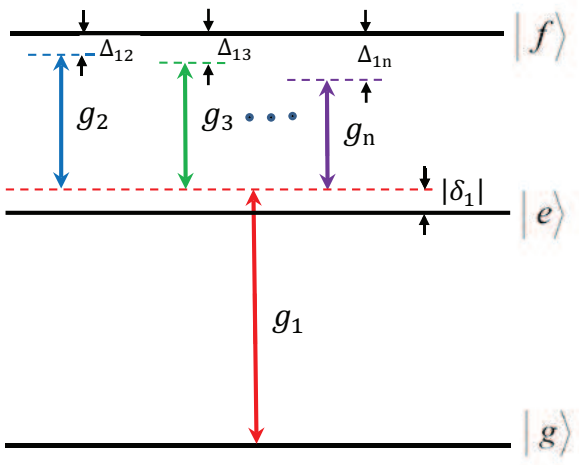


FIG. 2: (Color online) Cavity 1 is far-off resonant with the $|g\rangle \leftrightarrow |e\rangle$ transition of the qutrit with coupling strength g_1 and detuning $|\delta_1|$, while cavity l ($l = 2, 3, ..., n$) is far-off resonant with the $|e\rangle \leftrightarrow |f\rangle$ transition of the qutrit with coupling strength g_l and detuning $|\delta_l|$. Note that the detunings $|\delta_l|$ ($l = 2, 3, ..., n$) are not drawn to simplify the figure. From the figure, one can see $|\delta_1| = \omega_{c_1} - \omega_{eg}$, $|\delta_l| = \omega_{fe} - \omega_{c_l} = |\delta_1| + \Delta_{1l}$, and $\Delta_{1l} = \omega_{fg} - \omega_{c_1} - \omega_{c_l} > 0$. Here, ω_{c_1} (ω_{c_l}) is the frequency of cavity 1 (l); ω_{eg}, ω_{fe}, and ω_{fg} are the $|g\rangle \leftrightarrow |e\rangle$, $|e\rangle \leftrightarrow |f\rangle$, and $|g\rangle \leftrightarrow |f\rangle$ transition frequencies of the qutrit, respectively. The red vertical line represents the frequency ω_{c_1} of cavity 1, while the blue, green, ..., and purple vertical lines represent the frequency ω_{c_2} of cavity 2, the frequency ω_{c_3} of cavity 3,..., and the frequency ω_{c_n} of cavity n, respectively.

1-3 ns) adjusted by varying external control parameters (e.g., magnetic flux applied to the superconducting loop of a SC phase, transmon [52], Xmon [53], or flux qubit/qutrit [54]. In addition, the frequency of a microwave cavity or resonator can be rapidly adjusted with a few nanoseconds [55,56].

Under the above assumptions, the Hamiltonian of the whole system, in the interaction picture and after making the rotating-wave approximation (RWA), can be written as (in units of $\hbar = 1$)

$$H_{\rm I} = g_1(e^{-i\delta_1 t}\hat{a}_1\sigma_{eg}^{+} + h.c.) + \sum_{l=2}^{n} g_l(e^{i\delta_l t}\hat{a}_l\sigma_{fe}^{+} + h.c.), \tag{2}$$

where $\sigma_{eg}^{+} = |e\rangle\langle g|$, $\sigma_{fe}^{+} = |f\rangle\langle e|$, $\delta_1 = \omega_{c_1} - \omega_{eg}$, and $\delta_l = \omega_{fe} - \omega_{c_l}$. To simplify Fig. 2, the detunings δ_l ($l = 2, 3, ..., n$) are not drawn in Fig. 2, but their definitions are given in the caption of Fig. 2. The detunings δ_1 and δ_l have a relationship $|\delta_l| = |\delta_1| + \Delta_{1l}$, with

$\Delta_{1l} = \omega_{fg} - \omega_{c_1} - \omega_{c_l} > 0$ (Fig. 2). Here, $\hat{a}_1$ ($\hat{a}_l$) is the photon annihilation operator of cavity 1 (l), ω_{c_l} is the frequency of cavity l ($l = 2, 3, ..., n$); while ω_{fe}, ω_{eg}, and ω_{fg} are the $|e\rangle \leftrightarrow |f\rangle$, $|g\rangle \leftrightarrow |e\rangle$, and $|g\rangle \leftrightarrow |f\rangle$ transition frequencies of the qutrit, respectively.

Under the large-detuning conditions $|\delta_1| \gg g_1$ and $|\delta_l| \gg g_l$, the Hamiltonian (2) becomes [57]

$$\begin{aligned} H_{\rm e} = & \quad \lambda_1(\hat{a}_1^+\hat{a}_1|g\rangle\langle g| - \hat{a}_1\hat{a}_1^+|e\rangle\langle e|) \\ & - \sum_{l=2}^{n} \lambda_l(\hat{a}_l^+\hat{a}_l|e\rangle\langle e| - \hat{a}_l\hat{a}_l^+|f\rangle\langle f|) \\ & + \sum_{l=2}^{n} \lambda_{1l}(e^{-i\triangle_{1l}t}\hat{a}_1^+\hat{a}_l^+\sigma_{fg}^- + h.c.) \\ & + \sum_{k\neq l;k,l=2}^{n} \lambda_{kl}\left(e^{i\triangle_{kl}t}\hat{a}_k^+\hat{a}_l + h.c.\right)(|f\rangle\langle f| - |e\rangle\langle e|), \end{aligned} \tag{3}$$

where $\lambda_1 = g_1^2/|\delta_1|$, $\lambda_l = g_l^2/|\delta_l|$, $\lambda_{1l} = (g_1 g_l/2)(1/|\delta_1| + 1/|\delta_l|)$, $\lambda_{kl} = (g_k g_l/2)(1/|\delta_k| + 1/|\delta_l|)$, $\triangle_{kl} = |\delta_l| - |\delta_k| = \omega_{c_k} - \omega_{c_l}$, and $\sigma_{fg}^- = |g\rangle\langle f|$. In Eq. (3), the terms in the first two lines describe the photon number dependent stark shifts of the energy levels $|g\rangle$, $|e\rangle$ and $|f\rangle$, the terms in the third line describe the $|f\rangle \leftrightarrow |g\rangle$ coupling caused due to the cooperation of cavitie 1 and l, while the terms in the last line describe the coupling between cavities k and l. For $\triangle_{1l} \gg \{\lambda_1, \lambda_l, \lambda_{1l}\}$, the effective Hamiltonian $H_{\rm e}$ changes to [57]

$$\begin{aligned} H_{\rm e} = & \quad \lambda_1(\hat{a}^+\hat{a}|g\rangle\langle g| - \hat{a}\hat{a}^+|e\rangle\langle e|) \\ & - \sum_{l=2}^{n} \lambda_l(\hat{a}_l^+\hat{a}_l|e\rangle\langle e| - \hat{a}_l\hat{a}_l^+|f\rangle\langle f|) \\ & + \sum_{l=2}^{n} \chi_{1l}(\hat{a}_1\hat{a}_1^+\hat{a}_l\hat{a}_l^+|f\rangle\langle f| - \hat{a}_1^+\hat{a}_1\hat{a}_l^+\hat{a}_l|g\rangle\langle g|) \\ & + \sum_{k\neq l;k,l=2}^{n} \lambda_{kl}\left(e^{i\triangle_{kl}t}\hat{a}_k^+\hat{a}_l + h.c.\right)(|f\rangle\langle f| - |e\rangle\langle e|), \end{aligned} \tag{4}$$

where $\chi_{1l} = \lambda_{1l}^2/\Delta_{1l}$. Eq. (4) shows that each term is associated with the level $|g\rangle$, $|e\rangle$, or $|f\rangle$. When the levels $|e\rangle$ and $|f\rangle$ are initially not occupied, they will remain unpopulated under the Hamiltonian (4). This is because the Hamiltonian (4) does not induce either $|g\rangle \rightarrow |e\rangle$ transition or $|g\rangle \rightarrow |f\rangle$ transition. Thus, the effective Hamiltonian (4) reduces to

$$H_{\rm e} = \lambda_1\hat{n}_1|g\rangle\langle g| - \sum_{l=2}^{n} \chi_{1l}\hat{n}_1\hat{n}_l|g\rangle\langle g|, \tag{5}$$

where $\hat{n}_1 = \hat{a}_1^+\hat{a}_1$ and $\hat{n}_l = \hat{a}_l^+\hat{a}_l$ are the photon number operators for cavities 1 and l, respectively.

Suppose that the qutrit is initially in the ground state $|g\rangle$. It will remain in this state throughout the interaction as the Hamiltonian $H_{\rm e}$ cannot induce any transition for the qutrit. In this case, the Hamiltonian $H_{\rm e}$ is reduced to

$$\widetilde{H}_{\rm e} = H_0 + H_{\rm int}, \tag{6}$$

with

$$\begin{aligned} H_0 &= \lambda_1 \hat{n}_1, \\ H_{\rm int} &= -\sum_{l=2}^{n} \chi_{1l} \hat{n}_1 \hat{n}_l, \end{aligned} \tag{7}$$

which is the effective Hamiltonian governing the dynamics of the n cavities $(1, 2, ..., n)$.

Because of $[H_0, H_{\rm int}] = 0$, the unitary operator $U = e^{-i\widetilde{H}_{\rm e}t}$ can be written as

$$U = e^{-iH_0 t} \otimes e^{-iH_{\rm int}t} = U_1 \otimes \prod_{l=2}^{n} U_{1l}, \tag{8}$$

where U_1 is a unitary operator on cavity 1, while U_{1l} is a unitary operator on cavities 1 and l, given by

$$U_1 = \exp\left(-i\lambda_1 \hat{n}_1 t\right), \tag{9}$$

$$U_{1l} = \exp\left(i\chi_{1l} \hat{n}_1 \hat{n}_l t\right). \tag{10}$$

For a cqubit, the two logical states $|0\rangle$ and $|1\rangle$ are encoded with cat states of a cavity, i.e.,

$$\begin{aligned} |0\rangle &= N_\alpha^+(|\alpha\rangle + |-\alpha\rangle), \\ |1\rangle &= N_\alpha^-(|\alpha\rangle - |-\alpha\rangle), \end{aligned} \tag{11}$$

where $N_\alpha^\pm = 1/\sqrt{2(1 \pm e^{-2|\alpha|^2})}$ are the normalization coefficients. Because of $|\alpha\rangle = e^{-|\alpha|^2/2} \sum_{n=0}^{\infty} \frac{\alpha^n}{\sqrt{n!}} |n\rangle$ and $|-\alpha\rangle = e^{-|\alpha|^2/2} \sum_{n=0}^{\infty} \frac{(-\alpha)^n}{\sqrt{n!}} |n\rangle$, we have

$$\begin{aligned} |0\rangle &= \sum_{m=0}^{\infty} C_{2m} |2m\rangle, \\ |1\rangle &= \sum_{n=0}^{\infty} C_{2n+1} |2n+1\rangle, \end{aligned} \tag{12}$$

where $C_{2m} = 2N_\alpha^+ e^{-|\alpha|^2/2} \alpha^{2m} / \sqrt{(2m)!}$ and $C_{2n+1} = 2N_\alpha^- e^{-|\alpha|^2/2} \alpha^{2n+1} / \sqrt{(2n+1)!}$. Eq. (12) shows that the cat state $|0\rangle$ is orthogonal to the cat state $|1\rangle$, independent of α (except for $\alpha = 0$).

Based on Eq. (10) and Eq. (12), one can easily see that the unitary operation U_{1l} leads to the following state transformation

$$\begin{aligned}
U_{1l}|1_1 1_l\rangle_{ab} &= \sum_{n,n'=0}^{\infty} \exp[i(2n+1)(2n'+1)\chi_{1l}t] C_{2n+1} C_{2n'+1} |2n+1\rangle_1 |2n'+1\rangle_l, \\
U_{1l}|1_1 0_l\rangle &= \sum_{n,m\prime=0}^{\infty} \exp[i(2n+1)(2m')\chi_{1l}t] C_{2n+1} C_{2m'} |2n+1\rangle_1 |2m'\rangle_l, \\
U_{1l}|0_1 0_l\rangle &= \sum_{m,m'=0}^{\infty} \exp\left[i(2m)(2m')\chi_{1l}t\right] C_{2m} C_{2m'} |2m\rangle_1 |2m'\rangle_l, \\
U_{1l}|0_1 1_l\rangle &= \sum_{m,n'=0}^{\infty} \exp[i(2m)(2n'+1)\chi_{1l}t] C_{2m} C_{2n'+1} |2m\rangle_1 |2n'+1\rangle_l. \qquad (13)
\end{aligned}$$

For $\chi_{1l}t = \pi$, we have $\exp\left[i(2m)(2m')\chi_{1l}t\right] = \exp[i(2m)(2n'+1)\chi_{1l}t] = \exp[i(2m)(2n'+1)\chi_{1l}t] = 1$ but $\exp[i(2n+1)(2n'+1)\chi_{1l}t] = -1$. Thus, the state transformation (13) becomes

$$\begin{aligned}
U_{1l}|0_1 0_l\rangle &= |0_1 0_l\rangle, \\
U_{1l}|0_1 1_l\rangle &= |0_1 1_l\rangle, \\
U_{1l}|1_1 0_l\rangle &= |1_1 0_l\rangle, \\
U_{1l}|1_1 1_l\rangle &= -|1_1 1_l\rangle, \qquad (14)
\end{aligned}$$

which shows that the operator U_{1l} implements a universal controlled-phase gate on two cqubits 1 and l, described by $|0_1 0_l\rangle \to |0_1 0_l\rangle$, $|0_1 1_l\rangle \to |0_1 1_l\rangle$, $|1_1 0_l\rangle \to |1_1 0_l\rangle$, and $|1_1 1_l\rangle \to -|1_1 1_l\rangle$. It is obvious that the state transformation (14) can be simplified as

$$\begin{aligned}
U_{1l}|0_1 i_l\rangle|g\rangle &= |0_1 i_l\rangle|g\rangle \\
U_{1l}|1_1 i_l\rangle|g\rangle &= (-1)^{i_l} |1_1 i_l\rangle|g\rangle, \qquad (15)
\end{aligned}$$

where $i_l \in \{0,1\}$.

According to Eq. (15), it is easy to obtain the following state transformation

$$\begin{aligned}
\prod_{l=2}^{n} U_{1l} |0_1\rangle |i_2\rangle |i_3\rangle ... |i_n\rangle &= |0_1\rangle |i_2\rangle |i_3\rangle ... |i_n\rangle, \\
\prod_{l=2}^{n} U_{1l} |1_1\rangle |i_2\rangle |i_3\rangle ... |i_n\rangle &= |1_1\rangle (-1)^{i_2} (-1)^{i_3} ... (-1)^{i_n} |i_2\rangle |i_3\rangle ... |i_n\rangle. \qquad (16)
\end{aligned}$$

Now let us go back to the operator U_1. According to (9) and (12), this unitary operator leads to the following state transformation

$$\begin{aligned} U_1|0_1\rangle &= \sum_{m=0}^{\infty} \exp\left[-i(2m)\lambda_1 t\right] C_{2m}|2m\rangle_1, \\ U_1|1_1\rangle &= \sum_{n=0}^{\infty} \exp[-i(2n+1)\lambda_1 t] C_{2n+1}|2n+1\rangle_1. \end{aligned} \tag{17}$$

For $\lambda_1 t = 2\pi$, we have $\exp\left[-i(2m)\lambda_1 t\right] = \exp[-i(2n+1)\lambda_1 t] = 1$. Hence, Eq. (17) becomes

$$\begin{aligned} U_1|0_1\rangle &= |0_1\rangle, \\ U_1|1_1\rangle &= |1_1\rangle. \end{aligned} \tag{18}$$

Combining Eq. (16) and Eq. (18) leads to

$$\begin{aligned} U_1 \prod_{l=2}^{n} U_{1l} \left|1_1\right\rangle \left|i_2\right\rangle \left|i_3\right\rangle ... \left|i_n\right\rangle &= \left|1_1\right\rangle (-1)^{i_2} (-1)^{i_3} ... (-1)^{i_n} \left|i_2\right\rangle \left|i_3\right\rangle ... \left|i_n\right\rangle, \\ U_1 \prod_{l=2}^{n} U_{1l} \left|0_1\right\rangle \left|i_2\right\rangle \left|i_3\right\rangle ... \left|i_n\right\rangle &= \left|0_1\right\rangle \left|i_2\right\rangle \left|i_3\right\rangle ... \left|i_n\right\rangle. \end{aligned} \tag{19}$$

The result (19) shows that when the control cqubit 1 is in the state $|0\rangle$, nothing happens to the states of each of target cqubit $(2, 3, ..., n)$; however, when the control cqubit 1 is in $|1\rangle$, a phase flip (from sign + to −) happens to the state $|1\rangle$ of each of target cqubits $(2, 3, ..., n)$. Note that $U = U_1 \otimes \prod_{l=2}^{n} U_{1l}$ [see Eq. (8)]. Hence, a multi-target-qubit controlled phase gate, described by Eq. (1), is implemented with n cqubits $(1, 2, ..., n)$, after the above operation described by the unitary operator U.

From the description given above, one can see that the gate realization is based on a single unitary operator U which was obtained by starting with the original Hamiltonian (2). Hence, the gate is implemented with a single operation described by U. The qutrit remains in the ground state during the gate operation. Therefore, decoherence from the qutrit is greatly suppressed.

As shown above, the conditions $\chi_{1l} t = \pi$ (independent l) and $\lambda_1 t = 2\pi$ should be met. They turn out into $\chi_{1l} = \lambda_1/2$, which can be further written as

$$g_l = \frac{|\delta_l|}{|\delta_1| + |\delta_l|} \sqrt{2\Delta_{1l} |\delta_1|}. \tag{20}$$

This condition (20) can be readily satisfied by varying g_l or $|\delta_l|$ or both, given $|\delta_1|$. Note that the detuning $|\delta_l|$ can be adjusted by changing the frequency of cavity l, and the coupling

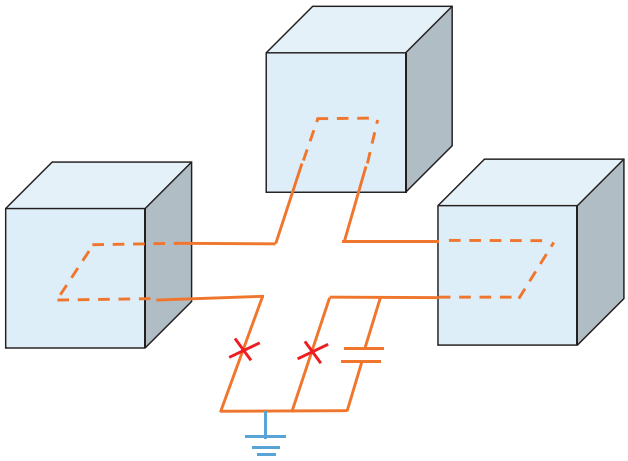


FIG. 3: (Color online) Setup for three 3D microwave cavities inductively coupled to a transmon qutrit. Electronic circuit of a transmon qutrit consists of two Josephson junctions and a capacitor.

strength g_l can be adjusted by a prior design of the sample with appropriate capacitance or inductance between the qutrit and cavity l [58,59].

Another point should be mentioned here. For circuit QED, the frequencies of cavities $(2, 3, ..., n)$ should be different in order to suppress the unwanted inter-cavity crosstalk. Because of $\Delta_{1l} = \omega_{fg} - \omega_{c_1} - \omega_{c_l}$ depending ω_{c_l}, the detuning Δ_{1l} would be different for cavities $(2, 3, ..., n)$ with different frequencies. However, for a cavity QED system consisting of cavities and a natural atom (the coupler), there does not exist the inter-cavity crosstalk. Thus, each of cavities $(2, 3, ..., n)$ can be allowed to have the same frequency, resulting in the same detuning Δ_{1l}. This would significantly reduce the experimental difficulty.

Before ending this section, we should point out that in quantum optics, the two cat states described by Eq. (11) are called even and odd coherent states, respectively. According to Ref. [60], the encoding (11) for a cat-state qubit works for a noise environment without phase damping or a noise environment where phase damping is not dominant.

III. POSSIBLE EXPERIMENTAL IMPLEMENTATION

For the sake of definitiveness, we give a brief discussion on the experimental feasibility of implementing a three-qubit controlled phase gate with one cqubit simultaneously controlling two target cqubits, by considering a setup of a SC transmon qutrit coupled to three 3D microwave cavities or resonators.

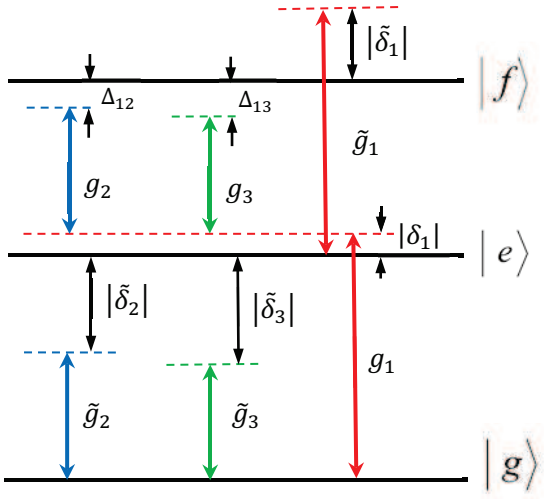


FIG. 4: (Color online) Illustration of the unwanted coupling between cavity 1 and the $|e\rangle \leftrightarrow |f\rangle$ transition of the qutrit (with coupling strength $\widetilde{g}_1$ and detuning $\left|\widetilde{\delta}_1\right|$) as well as the unwanted coupling between cavity l and the $|g\rangle \leftrightarrow |e\rangle$ transition of the qutrit (with coupling strength $\widetilde{g}_l$ and detuning $\left|\widetilde{\delta}_l\right|$) $(l = 2, 3)$. Here, $\left|\widetilde{\delta}_1\right| = \omega_{c_1} - \omega_{fe}$ and $\left|\widetilde{\delta}_l\right| = \omega_{eg} - \omega_{c_l}$ $(l = 2, 3)$. Other couplings depicted in the figure are needed, as described by the Hamiltonian (2) with $n = 3$. Note that the coupling of each cavity with the $|g\rangle \leftrightarrow |f\rangle$ transition of the qutrit is negligible because of the forbidden or very weak $|g\rangle \leftrightarrow |f\rangle$ transition [50,51].

From the description given above, one can see that the gate implementation involves the operation, described by the Hamiltonian (2). In reality, the inter-cavity crosstalk between cavities should be considered [61], and there exist the unwanted coupling of cavity 1 with the $|e\rangle \leftrightarrow |f\rangle$ transition and the unwanted coupling of cavities 2 and 3 with the $|g\rangle \leftrightarrow |e\rangle$ transition of the qutrit (Fig. 4). When these factors are taken into account, the Hamiltonian (2) becomes

$$\widetilde{H}_{\rm I} = H_{\rm I} + \Delta H + \varepsilon, \tag{21}$$

with

$$\begin{aligned} \Delta H \;=\; & \widetilde{g}_1(e^{-i\widetilde{\delta}_1 t}\hat{a}_1\sigma_{fe}^{+} + h.c.) \\ & + \sum_{l=2}^{3}\widetilde{g}_l(e^{i\widetilde{\delta}_l t}\hat{a}_l\sigma_{eg}^{+} + h.c.), \end{aligned} \tag{22}$$

$$\varepsilon = \sum_{k\neq l;k,l=1}^{3} g_{kl}(e^{-i\widetilde{\Delta}_{kl}t}\hat{a}_k\hat{a}_l^{+} + h.c.) \tag{23}$$

where $H_{\rm I}$ is the Hamiltonian (2) for $n=3$, ΔH is the Hamiltonian describing the unwanted coupling between cavity 1 and the $|e\rangle \leftrightarrow |f\rangle$ transition with coupling strength $\widetilde{g}_1$ and detuning $\widetilde{\delta}_1 = \omega_{c_1} - \omega_{fe}$ as well as the unwanted coupling between cavity l and the $|g\rangle \leftrightarrow |e\rangle$ transition with coupling strength $\widetilde{g}_l$ and detuning $\widetilde{\delta}_l = \omega_{eg} - \omega_{c_l}$ $(l = 2, 3)$ (Fig. 4); ε represents the inter-cavity crosstalk, where g_{kl} is the coupling strength between cavities k and l while $\widetilde{\triangle}_{kl} = \omega_{c_k} - \omega_{c_l}$ is the difference between the frequencies of cavities k and l $(k \neq l; k, l \in \{1, 2, 3\})$.

The dynamics of the lossy system is determined by

$$\begin{aligned}\frac{d\rho}{dt} = & -i[\widetilde{H}_{\rm I}, \rho] + \textstyle\sum_{l=1}^{3} \kappa_l \mathcal{L}[a_l] \\ & + \gamma_{eg}\mathcal{L}[\sigma_{eg}^{-}] + \gamma_{fe}\mathcal{L}[\sigma_{fe}^{-}] + \gamma_{fg}\mathcal{L}[\sigma_{fg}^{-}] \\ & + \sum_{j=e,f} \{\gamma_{\varphi j}(\sigma_{jj}\rho\sigma_{jj} - \sigma_{jj}\rho/2 - \rho\sigma_{jj}/2)\}, \end{aligned} \tag{24}$$

where $\widetilde{H}_{\rm I}$ is the full Hamiltonian given above, $\sigma_{eg}^{-} = |g\rangle\langle e|$, $\sigma_{fe}^{-} = |e\rangle\langle f|$, $\sigma_{fg}^{-} = |g\rangle\langle f|$, $\sigma_{jj} = |j\rangle\langle j| (j = e, f)$; and $\mathcal{L}[\xi] = \xi\rho\xi^{+} - \xi^{+}\xi\rho/2 - \rho\xi^{+}\xi/2$ with $\xi = a_l, \sigma_{eg}^{-}, \sigma_{fe}^{-}, \sigma_{fg}^{-}$. In addition, κ_l is the photon decay rate of cavity l $(l = 1, 2, 3)$, γ_{eg} is the energy relaxation rate for the level $|e\rangle$ of the qutrit, $\gamma_{fe}(\gamma_{fg})$ is the energy relaxation rate of the level $|f\rangle$ of the qutrit for the decay path $|f\rangle \longrightarrow |e\rangle(|g\rangle)$, and $\gamma_{\varphi j}$ is the dephasing rate of the level $|j\rangle (j = e, f)$ of the qutrit.

The fidelity of the operation is given by

$$\mathcal{F} = \sqrt{\langle\psi_{\rm id}|\rho|\psi_{\rm id}\rangle}, \tag{25}$$

where $|\psi_{\rm id}\rangle$ is the output state of an ideal system without dissipation, dephasing and crosstalk; while ρ is the final practical density operator of the system when the operation is performed in a realistic situation. The input state of the whole system is given by

$$\begin{aligned}|\psi_{\rm in}\rangle = & (c_0|000\rangle + c_1|001\rangle + c_2|010\rangle + c_3|011\rangle \\ & + c_4|100\rangle + c_5|101\rangle + c_6|110\rangle + c_7|111\rangle) \otimes |g\rangle . \end{aligned} \tag{26}$$

where the coefficients $c_0, c_1, ...,$and c_7 satisfy the normalization condition $\sum_{k=0}^{7} |c_k|^2 = 1$. Thus, the ideal output state is

$$\begin{aligned}|\psi_{\rm id}\rangle = & (c_0|000\rangle + c_1|001\rangle + c_2|010\rangle + c_3|011\rangle \\ & + c_4|100\rangle - c_5|101\rangle - c_6|110\rangle + c_7|111\rangle) \otimes |g\rangle . \end{aligned} \tag{27}$$

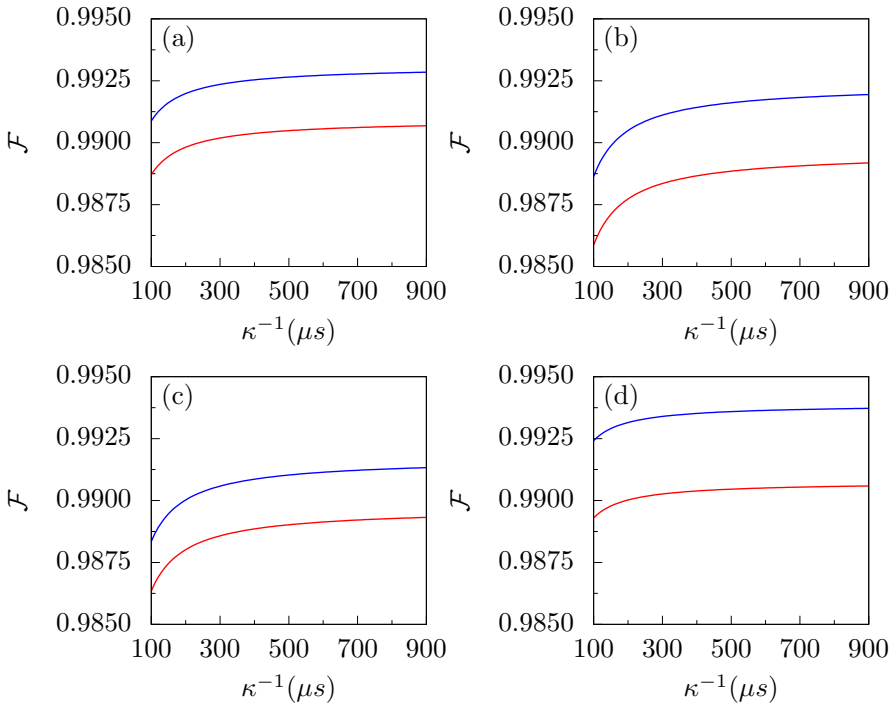


FIG. 5: (Color online) Fidelity versus κ^{-1}. The plots are drawn for $\alpha = 0.5$. Other parameters used in the numerical simulation are referred to the text. Blue curves are based on the effective Hamitonian (5) and considering decoherence and the inter-cavity crosstalk; while red curves are based on the full Hamiltonian (21) and considering decoherence and the inter-cavity crosstalk. (a) is plotted for $\gamma = \theta = \varphi = \pi/4$; (b) is for $\gamma = \theta = \varphi = \pi/3$; (c) is for $\gamma = \pi/2, \theta = \pi/4, \varphi = \pi/3$; while (d) is for $\gamma = \pi, \theta = \pi/3, \varphi = \pi/4$.

For simplicity, we choose

$$\begin{aligned} c_0 &= \cos\gamma\cos\theta\cos\varphi;\ \ c_4 = \sin\gamma\cos\theta\cos\varphi, \\ c_1 &= \cos\gamma\cos\theta\sin\varphi;\ \ c_5 = \sin\gamma\cos\theta\sin\varphi, \\ c_2 &= \cos\gamma\sin\theta\cos\varphi;\ \ c_6 = \sin\gamma\sin\theta\cos\varphi, \\ c_3 &= \cos\gamma\sin\theta\sin\varphi;\ \ c_7 = \sin\gamma\sin\theta\sin\varphi. \end{aligned} \tag{28}$$

In the following, we will consider the cases: (a) $\gamma = \theta = \varphi = \pi/4$; (b) $\gamma = \theta = \varphi = \pi/3$; (c) $\gamma = \pi/2, \theta = \pi/4, \varphi = \pi/3$; and (d) $\gamma = \pi, \theta = \pi/3, \varphi = \pi/4$; which correspond to four initial states.

For a transmon qutrit, the typical transition frequency between neighboring levels can be made as 3 to 15 GHz and the anharmonicity $100 \sim 500$ MHz of the level spacings has been

reported in experiments [62,63]. As an example, we thus consider $\omega_{eg}/2\pi = 6.5$ GHz and $\omega_{fe}/2\pi = 6.2$ GHz. By choosing $|\delta_1|/2\pi = 0.5$ GHz, $|\delta_2|/2\pi = 0.51$ GHz, and $|\delta_3|/2\pi = 0.52$ GHz, we have $\Delta_{12}/2\pi = 0.01$ GHz, $\Delta_{13}/2\pi = 0.02$ GHz, $\omega_{c_1}/2\pi = 7.0$ GHz, $\omega_{c_2}/2\pi = 5.69$ GHz, and $\omega_{c_3}/2\pi = 5.68$ GHz, for which we have $\widetilde{\Delta}_{12}/2\pi = 1.31$ GHz, $\widetilde{\Delta}_{23}/2\pi = 0.01$ GHz, and $\widetilde{\Delta}_{13}/2\pi = 1.32$ GHz. With the transition frequencies of the qutrit and the frequecies of the cavities given here, we have $\left|\widetilde{\delta}_1\right|/2\pi = 0.8$ GHz, $\left|\widetilde{\delta}_2\right|/2\pi = 0.81$ GHz, and $\left|\widetilde{\delta}_3\right|/2\pi = 0.82$ GHz. Other parameters used in the numerical simulation are: (i) $\gamma_{eg}^{-1} = 60$ μs, $\gamma_{fg}^{-1} = 150$ μs [64], $\gamma_{fe}^{-1} = 30$ μs, $\gamma_{\phi e}^{-1} = \gamma_{\phi f}^{-1} = 20$ μs, (ii) $g_1/2\pi = 35$ MHz, and (iii) $\alpha = 0.5$. Here, we consider a rather conservative case for decoherence time of the transmon qutrit because energy relaxation time with a range from 65 μs to 0.1 ms and dephasing time from 25 μs to 70 μs have been experimentally reported for a 3D superconducting transmon device [33,65,66]. According to Eq. (20), one can calculate the g_2 and g_3, which are $g_2/2\pi \sim 50.5$ MHz and $g_3/2\pi \sim 72.1$ MHz. For a transmon qutrit [50], one has $\widetilde{g}_1/2\pi \sim \sqrt{2}g_1/2\pi \sim 49.5$ MHz, $\widetilde{g}_2/2\pi \sim g_2/(2\pi\sqrt{2}) \sim 35.7$ MHz, and $\widetilde{g}_3/2\pi \sim g_3/(2\pi\sqrt{2}) \sim 41.6$ MHz. Note that the coupling constants chosen here are readily available because a coupling constant $\sim 2\pi \times 360$ MHz has been reported for a transmon device coupled to a microwave cavity [67]. We set $g_{kl} = 0.01 g_{\max}$, where $g_{\max} = \max\{g_1, g_2, g_3\} \sim 2\pi \times 72.1$ MHz, which can be achieved in experiments [33]. In addition, assume $\kappa_1 = \kappa_2 = \kappa_3 = \kappa$ for simplicity.

By solving the master equation (24), we numerically calculate the fidelity versus κ^{-1}, as depicted in Fig. 5. Fig. 5(a) is plotted for $\gamma = \theta = \varphi = \pi/4$. Fig. 5(b) is for $\gamma = \theta = \varphi = \pi/3$. Fig. 5(c) is for $\gamma = \pi/2, \theta = \pi/4, \varphi = \pi/3$. Fig. 5(d) is for $\gamma = \pi, \theta = \pi/3, \varphi = \pi/4$. In Fig. 5, the red curves are plotted by numerical simulations, based on the full Hamiltonians $\widetilde{H}_{\rm I}$ and by taking decoherence and the inter-cavity crosstalk into consideration. From the red curves, one can see that when $\kappa^{-1} \geq 300$ μs, fidelity exceeds: (i) 0.9902 for $\gamma = \theta = \varphi = \pi/4$; (ii) 0.9884 for $\gamma = \theta = \varphi = \pi/3$; (iii) 0.9886 for $\gamma = \pi/2, \theta = \pi/4, \varphi = \pi/3$; and (iv) 0.9903 for $\gamma = \pi, \theta = \pi/3, \varphi = \pi/4$. These results imply that the fidelity varies with different initial states of the three cavities, but a high fidelity can be obtained for the gate being performed in a realistic situation.

We also calculate the fidelity, based on the effective Hamiltonian $H_{\rm e}$ in Eq. (5) and by considering decoherence and the inter-cavity crosstalk (see the blue curves in Fig. 5). From the red curves and the bule curves in Fig. 5, it can be concluded that the fidelity for the gate performed in a realistic situation is slightly decreased by $0.2\% - 0.5\%$, when compared to

the case of the gate performed based on the effective Hamiltonian. This result implies that the approximations, which we made above for the effective Hamiltonian, are reasonable.

The gate operational time is estimated as ~ 0.41 μs for the parameters chosen above, which is much shorter than the decoherence times of the qutrit used in the numerical simulation and the cavity decay times (100 μs $-$ 900 μs) considered in Fig. 5. Note that lifetime ~ 1 ms of microwave photons has been experimentally demonstrated in a 3D resonator [46,68]. For the cavity frequencies given above and $\kappa^{-1} = 300$ μs, one has $Q_1 \sim 1.31 \times 10^7$ for cavity 1, $Q_2 \sim 1.07 \times 10^7$ for cavity 2, and $Q_3 \sim 1.07 \times 10^7$ for cavity 3, which are available because a high quality factor $Q = 3.5 \times 10^7$ of a 3D superconducting cavity has been experimentally reported [68]. The analysis here implies that high-fidelity realization of a quantum controlled phase gate with one cqubit simultaneously controlling two target cqubit is feasible with the present circuit QED technology.

IV. CONCLUSIONS

We have proposed a one-step method to realize an n-qubit controlled phase gate with one cat-state qubit simultaneously controlling $n-1$ target cat-state qubits, based on circuit QED. This method can be applied to implement the proposed gate with a wide range of physical systems, such as multiple microwave or optical cavities coupled to a single three-level natural or artificial atom. As shown above, this proposal has the following features: (i) During the gate operation, the qutrit remains in the ground state; thus decoherence from the qutrit is greatly suppressed; (ii) Because only one-step operation is needed and neither classical pulse nor measurement is required, the gate realization is simple; and (iii) The gate operation time is independent of the number of the cat-state qubits. Our numerical simulations show that high-fidelity implementation of a three-qubit controlled phase gate with one cat-state qubit simultaneously controlling two target cat-state qubits is feasible with current circuit QED technology. To the best of our knowledge, this work is the first to demonstrate the implementation of a multi-target-qubit controlled phase gate with cat-state qubits based on cavity- or circuit-QED. We hope that this work will stimulate experimental activities in the near future.

Acknowledgments

This work was supported in part by the NKRDP of China (Grant No. 2016YFA0301802) and the National Natural Science Foundation of China under Grant Nos. [11074062, 11374083,11774076]. This work was also supported by the Hangzhou-City grant for Quantum Information and Quantum Optics Innovation Research Team.

---

[1] D. Deutsch, Quantum theory, the Church-Turing principle and the universal quantum computer, Proc. R. Soc. London, Ser. A **400**, 97 (1985).

[2] P. W. Shor, in Proceedings of the 35th Annual Symposium on Foundations of Computer Science (IEEE Computer Society Press, Santa Fe, NM, 1994).

[3] L. K. Grover, Quantum mechanics helps in searching for a needle in a haystack, Phys. Rev. Lett. **79**, 325 (1997).

[4] A. Barenco et al., Elementary gates for quantum computation, Phys. Rev. A **52**, 3457 (1995).

[5] M. Mötöen, J. J. Vartiainen, V. Bergholm, and M. M. Salomaa, Quantum circuits for general multiqubit gates, Phys. Rev. Lett. **93**, 130502 (2004).

[6] Y. Liu, G. L. Long, and Y. Sun, Analytic one-bit and CNOT gate constructions of general n-qubit controlled gates, Int. J. Quantum Inform. **6**, 447 (2008).

[7] J. K. Pachos and P. L. Knight, Quantum Computation with a One-dimensional optical lattice, Phys. Rev. Lett. **91**, 107902 (2003).

[8] H. Ollivier and P. Milman, Proposal for realization of a Toffoli gate via cavity-assisted collision, quant-ph/0306064.

[9] J. Zhang, W. Liu, Z. Deng, Z. Lu, and G. L. Long, Modularization of multi-qubit controlled phase gate and its NMR implementation, J. Opt. B: Quantum Semiclass. Opt. **7**, 22(2005).

[10] A. Fedorov, L. Steffen, M. Baur, da SilvaMP, and A. Wallraff, Implementation of a Toffoli gate with superconducting circuits, Nature **481**, 170 (2012).

[11] L. M. Duan, B. Wang, and H. J. Kimble, Robust quantum gates on neutral atoms with cavity-assisted photon-scattering, Phys. Rev. A **72**, 032333 (2005).

[12] X. Wang, A. Sørensen, and K. Mølmeret, Multibit gates for quantum computing, Phys. Rev. Lett. **86**, 3907 (2001).

[13] X. Zou, Y. Dong, and G. C. Guo, Implementing a conditional z gate by a combination of resonant interaction and quantum interference, Phys. Rev. A **74**, 032325 (2006).

[14] C. P. Yang and S. Han, n-qubit-controlled phase gate with superconducting quantum-interference devices coupled to a resonator, Phys. Rev. A **72**, 032311 (2005).

[15] C. P. Yang and S. Han, Realization of an n-qubit controlled-U gate with superconducting quantum interference devices or atoms in cavity QED, Phys. Rev. A **73**, 032317 (2006).

[16] W. L. Yang, Z. Q. Yin, Z. Y. Xu, M. Feng, and J. F. Du, One-step implementation of multi-qubit conditional phase gating with nitrogen-vacancy centers coupled to a high-Q silica microsphere cavity, Appl. Phys. Lett. **96**, 241113 (2010).

[17] S. B. Zheng, Implementation of Toffoli gates with a single asymmetric Heisenberg XY interaction, Phys. Rev. A **87**, 042318 (2013).

[18] T. Monz *et al.*, Realization of the quantum Toffoli gate with trapped ions, Phys. Rev. Lett. **102**, 040501 (2009).

[19] H. R. Wei and F. G. Deng, Universal quantum gates for hybrid systems assisted by quantum dots inside double-sided optical microcavities, Phys. Rev. A **87**, 022305 (2013).

[20] H. W. Wei and F. G. Deng, Scalable quantum computing based on stationary spin qubits in coupled quantum dots inside double-sided optical microcavities, Sci. Rep. **4**, 7551 (2014).

[21] M. Hua, M. J. Tao, and F. G. Deng, Universal quantum gates on microwave photons assisted by circuit quantum electrodynamics, Phys. Rev. A **90**, 012328 (2014).

[22] M. Hua, M. J. Tao, and F. G. Deng, Fast universal quantum gates on microwave photons with all-resonance operations in circuit QED, Scientific Reports **5**, 9274 (2015).

[23] C. P. Yang, Y. X. Liu, and F. Nori, Phase gate of one qubit simultaneously controlling n qubits in a cavity, Phys. Rev. A **81**, 062323 (2010).

[24] C. P. Yang, S. B. Zheng, and F. Nori, Multiqubit tunable phase gate of one qubit simultaneously controlling n qubits in a cavity, Phys. Rev. A **82**, 062326 (2010).

[25] C. P. Yang, Q. P. Su, F. Y. Zhang, and S. B. Zheng, Single-step implementation of a multiple-target-qubit controlled phase gate without need of classical pulses, Opt. Lett. **39**, 3312 (2014).

[26] H. F. Wang, A. D. Zhu, and S. Zhang, One-step implementation of a multiqubit phase gate with one control qubit and multiple target qubits in coupled cavities, Optics Letters **39**, 1489 (2014).

[27] T. Liu, X. Z. Cao, Q. P. Su, S. J. Xiong, and C. P. Yang, Multi-target-qubit unconventional

geometric phase gate in a multicavity system, Scientific Reports **6**, 21562 (2016).

[28] N. Ofek, A. Petrenko, R. Heeres, P. Reinhold, Z. Leghtas, B. Vlastakis, Y. Liu, L. Frunzio, S. M. Girvin, and L. Jiang et al., Extending the lifetime of a quantum bit with error correction in superconducting circuits, Nature **536**, 441 (2016).

[29] M. Mirrahimi, Z. Leghtas, V. V. Albert, S. Touzard, R. J. Schoelkopf, L. Jiang, and M. H. Devoret, Dynamically protected cat-qubits: a new paradigm for universal quantum computation, New J. Phys. **16**, 045014 (2014).

[30] S. E. Nigg, Deterministic hadamard gate for microwave cat-state qubits in circuit QED. Phys. Rev. A **89**, 022340 (2014).

[31] C. P. Yang, Q. P. Su, S. B. Zheng, F. Nori, and S. Han, Entangling two oscillators with arbitrary asymmetric initial states, Phys. Rev. A **95**, 052341 (2017).

[32] R. W. Heeres, P. Reinhold, N. Ofek, L. Frunzio, L. Jiang, M. H. Devoret, and R. J. Schoelkopf, Implementing a universal gate set on a logical qubit encoded in an oscillator, arXiv:1608.02430.

[33] C. Wang, Y. Y. Gao, P. Reinhold, R. W. Heeres, N. Ofek, K. Chou, C. Axline, M. Reagor, J. Blumoff, and K. M. Sliwa et al., A Schrodinger cat living in two boxes, Science **352**, 1087 (2016).

[34] C.P. Yang, S. I. Chu, and S. Han, Possible realization of entanglement, logical gates, and quantum-information transfer with superconducting-quantum-interference-device qubits in cavity QED, Phys. Rev. A **67**, 042311 (2003).

[35] J. Q. You, and F. Nori, Quantum information processing with superconducting qubits in a microwave field, Phys. Rev. B **68**, 064509 (2003).

[36] A. Blais, R. S. Huang, A. Wallraf, S. M. Girvin, and R. J. Schoelkopf, Cavity quantum electrodynamics for superconducting electrical circuits: An architecture for quantum computation, Phys. Rev. A **69**, 062320 (2004).

[37] J. Q. You and F. Nori, Superconducting circuits and quantum information, Phys. Today **58**, 42 (2005).

[38] J. Clarke and F. K. Wilhelm, Superconducting quantum bits, Nature **453**, 1031 (2008).

[39] J. Q. You and F. Nori, Atomic physics and quantum optics using superconducting circuits, Nature **474**, 589 (2011).

[40] Z. L. Xiang, S. Ashhab, J. Q. You, and F. Nori, Hybrid quantum circuits: Superconducting circuits interacting with other quantum systems. Rev. Mod. Phys. **85**, 623 (2013).

[41] X. Gu, A. F. Kockum, A. Miranowicz, Y. X. Liu, and F. Nori, Microwave photonics with superconducting quantum circuits. Phys. Rep. **718-719**, pp. 1-102 (2017).

[42] M. AbuGhanem, A. H. Homid, and M. Abdel-Aty, Cavity control as a new quantum algorithms implementation treatment, Front. Phys. **13**, 130303 (2018).

[43] H. P. Cui, Y. Shan, J. Zou, and B. Shao, Entanglement reciprocation between two charge qubits and two-cavity field, Front. Phys. China **3**, 258 (2008).

[44] P. B. Li, Y. C. Liu, S. Y. Gao, Z. L. Xiang, P. Rabl, Y. F. Xiao, and F. L. Li, Hybrid quantum device based on NV centers in diamond nanomechanical resonators plus superconducting waveguide cavities, Phys. Rev. Applied **4**, 044003 (2015).

[45] P. B. Li, S. Y. Gao, and F. L. Li, Engineering two-mode entangled states between two superconducting resonators by dissipation, Phys. Rev. A **86**, 012318 (2012).

[46] M. Šašura and V. Buzek, Multiparticle entanglement with quantum logic networks: Application to cold trapped ions, Phys. Rev. A **64**, 012305 (2001).

[47] F. Gaitan, Quantum error correction and fault tolerant quantum computing (CRC Press, USA, 2008).

[48] T.BethandM.Rötteler, Quantum information (Springer,Berlin, 2001), Vol. 173, Ch. 4, p. 96.

[49] S. L. Braunstein, V. Buzek, and M. Hillery, Quantum-information distributors: Quantum network for symmetric and asymmetric cloning in arbitrary dimension and continuous limit, Phys. Rev. A **63**, 052313 (2001).

[50] J. Koch, T. M. Yu, J. Gambetta, A. A. Houck, D. I. Schuster, J. Majer, A. Blais, M. H. Devoret, S. M. Girvin, and R. J. Schoelkopf, Charge-insensitive qubit design derived from the Cooper pair box, Phys. Rev. A **76**, 042319 (2007).

[51] D. Sank et al., Measurement-Induced State Transitions in a Superconducting qubit: Beyond the rotating wave approximation, Phys . Rev. Lett. **117**, 190503 (2016).

[52] P. J. Leek, S. Filipp, P. Maurer, M. Baur, R. Bianchetti, J. M. Fink, M. Göppl, L. Steffen, and A. Wallraff, Using sideband transitions for two-qubit operations in superconducting circuits, Phys. Rev. B **79**, 180511 (2009).

[53] R. Barends, J. Kelly, A. Megrant, D. Sank, E. Jeffrey, Y. Chen, Y. Yin, B. Chiaro, J. Mutus, and C. Neill *et al.*, Coherent Josephson qubit suitable for scalable quantum integrated circuits, Phys. Rev. Lett. **111**, 080502 (2013).

[54] M. Neeley, M. Ansmann, R. C. Bialczak, M. Hofheinz, N. Katz, Erik Lucero, A. O'Connell,

H. Wang, A. N. Cleland and J. M. Martinis, Process tomography of quantum memory in a Josephson-phase qubit coupled to a two-level state, Nat. Phys. **4**, 523 (2008).

[55] M. Sandberg, C. M. Wilson, F. Persson, T. Bauch, G. Johansson, V. Shumeiko, T. Duty, and P. Delsing, Tuning the field in a microwave resonator faster than the photon lifetime, Appl. Phys. Lett. **92**, 203501 (2008).

[56] Z. L. Wang, Y. P. Zhong, L. J. He, H. Wang, J. M. Martinis, A. N. Cleland, and Q. W. Xie, Quantum state characterization of a fast tunable superconducting resonator, Appl. Phys. Lett. **102**, 163503 (2013).

[57] D. F. James and J. Jerke, Effective hamiltonian theory and its applications in quantum information, Can. J. Phys. **85**, 625 (2007).

[58] Qi-Ping Su, H. H. Zhu, L. Yu, Y. Zhang, S. J. Xiong, J. M. Liu, and C. P. Yang, Generating double NOON states of photons in circuit QED, Phys. Rev. A **95**, 022339 (2017).

[59] C. P. Yang, Q. P. Su, S.. B. Zheng, and S. Han, One-step transfer or exchange of arbitrary multipartite quantum states with a single-qubit coupler, Phys. Rev. B **92**, 054509 (2015).

[60] Y. X. Liu, S. K. Özdemir, A. Miranowicz, and N. Imoto, Kraus representation of a damped harmonic oscillator and its application, Phys. Rev. A **70**, 042308 (2004).

[61] C. P. Yang, Q. P. Su, S. B. Zheng, and F. Nori, Crosstalk-insensitive method for simultaneously coupling multiple pairs of resonators, Phys. Rev. A **93**, 042307 (2016).

[62] J. A. Schreier, A. A. Houck, J. Koch, D. I. Schuster, B. R. Johnson, J. M. Chow, J. M. Gambetta, J. Majer, L. Frunzio, M. H. Devoret, S. M. Girvin, and R. J. Schoelkopf, Suppressing charge noise decoherence in superconducting charge qubits, Phys. Rev. B **77**, 180502(R) (2008).

[63] T. Niemczyk, F. Deppe, H. Huebl, E. P. Menzel, F. Hocke, M. J. Schwarz, J. J. Garcia-Ripoll, D. Zueco, T. Hümmer, and E. Solano *et al.*, Circuit quantum electrodynamics in the ultrastrong-coupling regime. Nat. Phys. **6**, 772 (2010).

[64] For a transmon qutrit, the $|g\rangle \leftrightarrow |f\rangle$ transition is much weaker than those of the $|g\rangle \leftrightarrow |e\rangle$ and $|e\rangle \leftrightarrow |f\rangle$ transitions. Thus, we have $\gamma_{fg}^{-1} \gg \gamma_{eg}^{-1}, \gamma_{fe}^{-1}$.

[65] C. Rigetti, S. Poletto, J. M. Gambetta, B. L. T. Plourde, J. M. Chow, A. D. Corcoles, J. A. Smolin, S. T. Merkel, J. R. Rozen, and G. A. Keefe *et al.*, Superconducting qubit in waveguide cavity with coherence time approaching 0.1 ms, Phys. Rev. B **86**, 100506(R) (2012).

[66] M. J. Peterer, S. J. Bader, X. Jin, F. Yan, A. Kamal, T. J. Gudmundsen, P. J. Leek, T. P.

Orlando, W. D. Oliver, and S. Gustavsson, Coherence and decay of higher energy levels of a superconducting transmon qubit. Phys. Rev. Lett. **114**, 010501 (2015).

[67] A. Fedorov, L. Steffen, M. Baur, M. P. da Silva, and A. Wallraff, Implementation of a Toffoli gate with superconducting circuits, Nature **481**, 170 (2011).

[68] M. Reagor, W. Pfaff, C. Axline, R. W. Heeres, N. Ofek, K. Sliwa, E. Holland, C. Wang, J. Blumoff, and K. Chou *et al.*, A quantum memory with near-millisecond coherence in circuit QED, Phys. Rev. B **94**, 014506 (2016).